Available online at www.sciencedirect.com
SCIENCE DIRECT®
Thermochimica Acta 433 (2005) 105–115
thermochimica acta
www.elsevier.com/locate/tca

Thermal study of HNIW (CL-20)

Richard Turcotte*, Marie Vachon, Queenie S.M. Kwok, Ruiping Wang, David E.G. Jones

Canadian Explosives Research Laboratory, Natural Resources Canada, 555 Booth Street, Ottawa, Ont., Canada K1A 0G1

Received 4 February 2005; accepted 14 February 2005
Available online 17 March 2005

Abstract

The thermal properties of the energetic material 2,4,6,8,10,12-hexanitro-2,4,6,8,10,12-hexaaza-tetracyclo-[5.5.0.0^{5,9}.0^{3,11}]-dodecane (HNIW), also known as CL-20, have been investigated by DSC, TG, ARC, HFC and simultaneous TG–DTA–FTIR–MS.

The solid–solid phase transitions and the reversibility of these phase transitions were explored using DSC. A heating rate study was performed and the DSC traces show the possibility of a multi-step thermal decomposition of CL-20. The enthalpies of reaction and onset temperatures were determined for various heating rates. The kinetic parameters were found by means of the ASTM E698 method and were verified by ageing experiments. A model-free kinetic (MFK) analysis was performed on the DSC heating rate results.

TG experiments were conducted to investigate the effects of various heating rates on the mass loss of CL-20 and its onset temperature. The TG results were analyzed using MFK and ASTM E1641 methods.

ARC measurements were performed to investigate the thermal stability of CL-20. The thermal behaviour of CL-20 at various pressures of argon was studied by heat flux calorimetry (HFC).

The gaseous products from the decomposition of CL-20 were determined by simultaneous TG–DTA–FTIR–MS experiments in air and in helium. The thermal stability at different isothermal temperatures (190, 195, 200 and 205 °C) was studied, using the same technique.

Keywords: Thermal analysis; CL-20; DSC; TG; TG–DTA–FTIR–MS; HFC; ARC

1. Introduction

According to the literature, addition of 2,4,6,8,10,12-hexanitro-2,4,6,8,10,12-hexaaza-tetracyclo-[5.5.0.0^{5,9}.0^{3,11}]-dodecane (HNIW or CL-20) to propellants or explosives is expected to increase the performance parameters such as specific impulse, ballistics and detonation velocity. Thus, it could possibly replace various explosive compounds such as RDX and HMX to produce high performance explosives with adequate vulnerability characteristics [1–3].

Compared to other nitramines, CL-20 has six N–NO_2 groups in its polycyclic structure (RDX and HMX have three and four N–NO_2 groups respectively), resulting in an increase in both density and heat of formation [4]. Six different polymorphs (α to ζ) of CL-20 have been identified [5,6]; the ε-phase has the highest stability at ambient temperature [6]. When heated to high temperatures in the DSC, two major conversions occur in CL-20: a solid–solid phase transition from $\varepsilon \rightarrow \gamma$ polymorphs ($T \approx 160$–$170\,^{\circ}C$) [1,4], followed by the thermal decomposition of the γ polymorph ($T > 210\,^{\circ}C$) [1,4,7].

CL-20 displays an interesting behaviour during its decomposition as both heating rate [4] and isothermal (see below) studies have evidenced a multi-step process. In previous isothermal TG studies somewhat contradictory results were reported. In an early study, Patil and Brill [8] studied the thermal decomposition of β-HNIW in the temperature range 190–204 °C. They reported that the rate of decomposition could be fitted equally well with a power rate law with $n = 1$ and 2, but that the same data could not be fitted using an autocatalytic model. In more recent work, performed in a

* Corresponding author. Tel.: +1 613 9965130; fax: +1 613 9951230.
E-mail address: richard.turcotte@nrcan-rncan.gc.ca (R. Turcotte).

0040-6031/$ – see front matter © 2005 Elsevier B.V. All rights reserved.
doi:10.1016/j.tca.2005.02.021

similar temperature range, it was shown that the data for the decomposition of the ε, α, and γ polymorphs could be well described by a first-order equation with autocatalysis [4,9–12]. Yet, in another recent isothermal TG study [7] performed in the 210–220 °C interval, the authors have reported that the best overall linear correlation was obtained using the Avrami–Erofeev equation. In this latter case, the polymorphic structure of the sample of CL-20 was not specified.

Some of the gaseous products from the decomposition of CL-20 (CO_2, N_2O, NO_2, NO, CO, HCN) were previously observed by FTIR [4,7].

This paper includes a detailed study of the following: kinetic parameters by DSC, thermal decomposition and mass loss by TG, thermal behaviour and identification of evolved gases by simultaneous TG–DTA–FTIR–MS, thermal decomposition by HFC, and thermal stability data by ARC.

2. Experimental

2.1. Materials

The CL-20 tested was supplied by ATK Thiokol Propulsion and was certified to be >95% ε-phase using FTIR. The chemical purity provided by the manufacturers was 99.9%.

2.2. Differential scanning calorimetry (DSC)

A TA Instruments 2910 DSC was used for studying the thermal properties of CL-20. The CL-20 samples were placed in aluminium pans with laser-drilled pinhole (75 μm) lids. Pinhole pans were used in this study, because both hermetic pans and glass ampoules gave unsatisfactory results due to the very energetic behaviour of CL-20. Dry, oxygen-free nitrogen was used to purge the DSC at a rate of 50 mL min^{-1}.

When conducting experiments to study the phase transitions, sample sizes of about 5 mg were used to increase the sensitivity and to obtain more accurate results from the instrument in that region of interest. Two sets of experiments were conducted to study the solid–solid phase transition of CL-20. For the first set, the samples were heated at 5 °C min^{-1} from 30 to 190 °C. For the second set of experiments, they were heated at 5 °C min^{-1} from 30 to 140 °C and then held isothermally at 140 °C for 60 min. After this isothermal period, they were cooled down to 100 °C and reheated to 190 °C at a rate of 5 °C min^{-1}.

In order to derive kinetic information, samples were heated from 30 to 300 °C using heating rates (β) ranging from 1 to 10 °C min^{-1}, following the ASTM E698 method [13]. Sample sizes of about 0.2 mg were employed for these experiments.

Temperature and heat flow calibrations using indium, tin and lead standards were performed prior to the experiments according to ASTM E967 [14] and ASTM E968 [15], respectively.

2.3. Thermogravimetry (TG)

A TA Instruments 2950 TG instrument was used to measure the sample mass loss during a heating rate study. Samples of about 1 mg were placed in a platinum pan, in a flow of dry nitrogen (100 mL min^{-1}, split 60:40 between the furnace and the balance). Following ASTM E1641 [16], CL-20 was heated from 30 to 300 °C using several heating rates between 0.5 and 10 °C min^{-1}. Prior to the experiments, the temperature was calibrated using the Curie point magnetic method with SRM nickel [17]. A mass calibration was also performed according to ASTM method E2040 [18].

2.4. Simultaneous TG–DTA–FTIR–MS

TG–DTA–FTIR–MS experiments were carried out using a TA Instruments simultaneous TG–DTA 2960 module (SDT) coupled to a Bomem MB100 FTIR Spectrometer and a Balzers Thermostar GSD300 quadrupole Mass Spectrometer. This system was already described in detail elsewhere [19]. Experiments were conducted in helium and air at a purge rate of 50 mL min^{-1}. Approximately 5 mg of sample and reference material (platinum foil) were placed in separate alumina pans. Both isothermal and heating rate studies were conducted on CL-20. For isothermal runs, the samples were heated at 20 °C min^{-1} to the desired temperature (190, 195, 200 and 205 °C) and maintained isothermally for time periods ranging from 200 to 400 min. For the heating rate studies, CL-20 was heated from 30 to 300 °C at 2, 5 or 10 °C min^{-1}.

TG mass, DTA baseline and temperature calibrations (indium and aluminium) were conducted prior to the experiments [14].

2.5. Heat flux calorimetry (HFC)

A modified Setaram C-80 heat flux calorimeter (HFC) [20] was used to study the thermal decomposition of CL-20 at atmospheric and elevated pressure of argon (7.4 MPa). About 50 mg of CL-20 were contained in an alumina liner and heated from room temperature to 300 °C at a rate of 0.3 °C min^{-1}. An equivalent mass of sapphire was contained in another liner and placed into the reference cavity of the calorimeter.

The system was leak tested prior to each run. The calorimeter was calibrated for temperature using indium and tin.

2.6. Accelerating rate calorimetry (ARC)

A Thermal Hazard Technology instrument was used to determine the thermal stability of CL-20. Samples of about 0.25 g of CL-20 were placed in a spherical (2.54 cm i.d.) thin-wall (0.9 mm) titanium vessel with a volume of 10 cm^3. Prior to each experiment, a high-pressure leak test was carried out at about 4.1 MPa. The ARC experiments were conducted at

ambient pressure of argon. The standard "heat-wait-search" procedure was used for these measurements [21]. The temperature of the system was raised by 5 °C steps. At each step, the system was kept adiabatic for a 'wait' period until thermal transients disappeared and then placed in 'search' mode, looking for an exotherm (self-heating rate ≥0.02 °C min^{-1}). ARC experiments were started at 50 °C and stopped automatically when the self-heating rate of the sample exceeded 5 °C min^{-1}.

3. Results

3.1. Differential scanning calorimetry (DSC)

Fig. 1 illustrates the thermal behaviour of CL-20 in nitrogen when heated in a pinhole pan from 30 to 300 °C at a heating rate of 5 °C min^{-1}. At about 160 °C, a solid–solid phase transition is detected as shown by the endothermic peak (see details in Fig. 2a), followed by the thermal decomposition of CL-20 starting around 210 °C.

3.1.1. Phase transition

The DSC curve in Fig. 2a demonstrates an endothermic behaviour of CL-20 with an onset temperature (first departure from the baseline) of $T_o = 141 \pm 1$ °C, and a peak temperature, $T_p = 162 \pm 1$ °C. Two endothermic peaks can be clearly observed, suggesting a two-step phase transition. In previous DSC work [4], only a single peak assigned to the conversion of $\varepsilon \rightarrow \gamma$ phase was detected at about $T_p = 171$ °C (in an argon atmosphere). Since CL-20 has four stable polymorphs (α, β, ε, γ) under ambient conditions [4], such differences may be due to the purity in ε-CL-20. Since no thermal data for the conversion of other polymorphs could be found in the literature, the lower temperature peak, in Fig. 2a cannot be assigned at this stage.

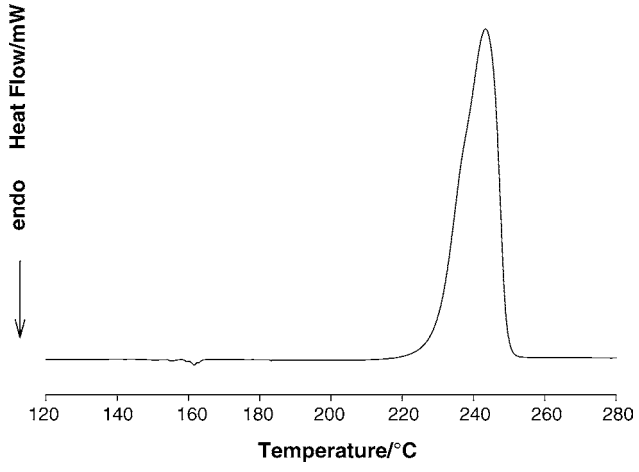

Fig. 1. Thermal behaviour of CL-20: DSC, 0.193 mg, 5 °C min^{-1}, pinhole pan, in nitrogen.

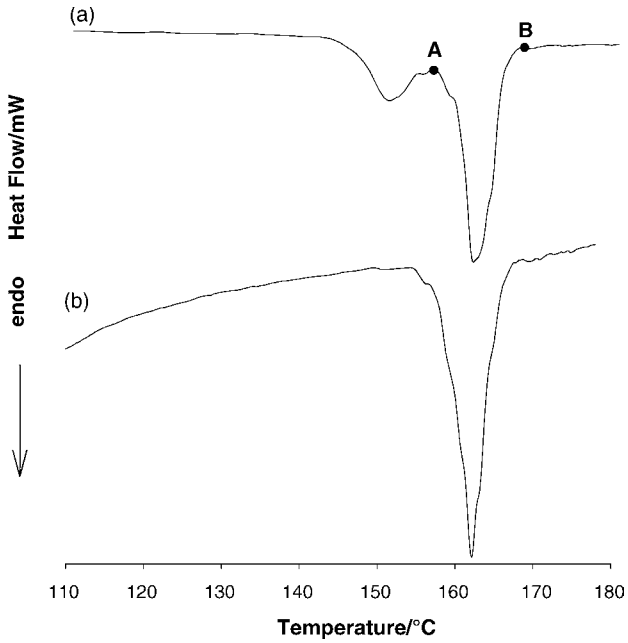

Fig. 2. Endothermic phase transition of CL-20: DSC, 5 °C min^{-1}, pinhole pan, in nitrogen: (a) 0.2 mg heated from 30 to 190 °C; (b) 5 mg with a 1 h isothermal step at 140 °C.

The integration of the endothermic peak between points A and B in Fig. 2a ($\varepsilon \rightarrow \gamma$), provides an enthalpy change of 13.5 ± 0.5 J g^{-1}, while integration of the complete endothermic structure leads to $\Delta H = 18 \pm 1$ J g^{-1}. These figures should be compared to $\Delta H = 16.54$ J g^{-1} reported by Löbbecke et al. [4] for a single endothermic peak with $T_o = 164$ °C and $T_p = 171$ °C. A mass loss of CL-20 (0.12 ± 0.07%) was observed after the runs.

Additional experiments were conducted to investigate these observed differences. The samples were heated at 5 °C min^{-1} to 140 °C and held isothermally at that temperature for 60 min. They were then cooled down at 5 °C min^{-1} to 100 °C and reheated to 190 °C at 5 °C min^{-1}. As seen from Fig. 2b, this extra isothermal step allows the sample to rearrange its structure before it reaches the phase transition. This structural rearrangement results in a single endothermic peak with an onset temperature of $T_o = 155 \pm 1$ °C and a peak temperature of $T_p = 162 \pm 1$ °C. The ΔH for this single endothermic peak is found to be 11.7 ± 0.5 J g^{-1}. Such behaviour demonstrates that prolonged storage of CL-20 at elevated temperature may induce phase instabilities.

Finally, another test method was carried out to determine if the observed phase transition is reversible. The samples (5.0 mg) were heated in aluminium pinhole (75 μm) pans from 30 to 190 °C at 5 °C min^{-1} and then cooled down to 80 °C using a 5 °C min^{-1} cooling rate. Fig. 3 shows no detectable transition on cooling. Therefore the phase transition of CL-20 observed in the heating cycle is irreversible on cooling under the experimental conditions used. A mass loss of 0.8 ± 0.3% was observed after the experiments.

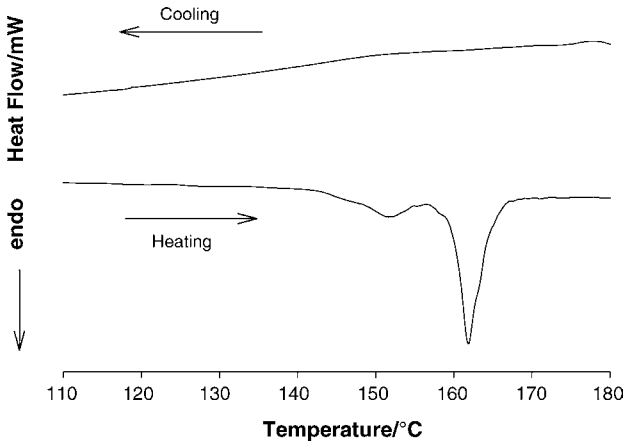

Fig. 3. Study of the reversibility of the phase transition of CL-20 by heating and cooling in DSC experiments.

3.1.2. Thermal decomposition

The ASTM method E698 [13] was used to determine the Arrhenius parameters for the thermal decomposition of CL-20. In order to calculate the pre-exponential factor (Z), it was assumed that the decomposition followed first-order kinetics. The DSC curves obtained at various heating rates are shown in Fig. 4. It is seen that the exothermic peaks are complex in nature and indicate a multi-step decomposition process. The thermal curves suggest two reaction zones: one with a relatively lower rate and a second with a relatively higher rate.

CL-20 loses $90 \pm 3\%$ of its mass when heated to 300 °C in a pinhole pan. The enthalpies of decomposition of CL-20 at different heating rates were determined by integrating the area under the exothermic peaks of Fig. 4, assuming a linear baseline. The average enthalpy of decomposition of CL-20 is $-2.9 \pm 0.3\,\mathrm{kJ\,g^{-1}}$. This value is in agreement with the value of $\Delta H = -2.59 \pm 0.07\,\mathrm{kJ\,g^{-1}}$ obtained in an earlier similar study [4].

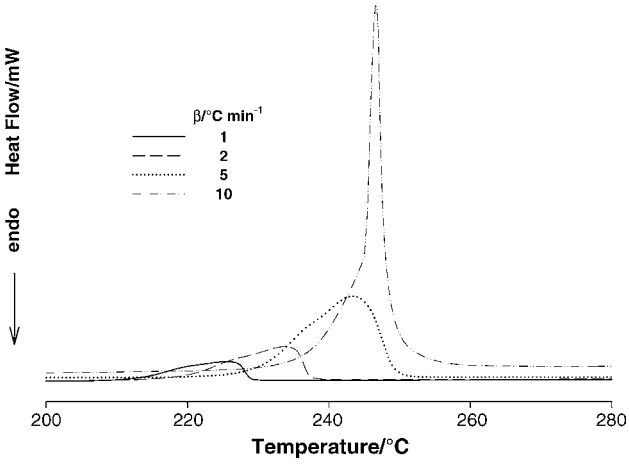

Fig. 4. Effect of various heating rates on the thermal decomposition of CL-20: DSC, ~0.2 mg.

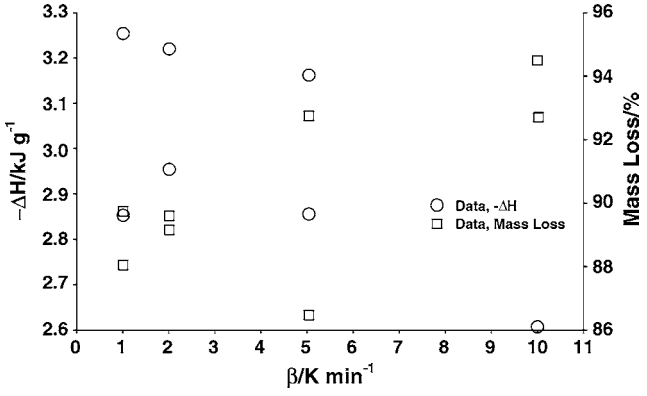

Fig. 5. Dependence of enthalpy of decomposition ($-\Delta H$) and mass loss on heating rate in DSC study.

The dependency of ΔH and the observed mass loss on β is shown in Fig. 5. Even though the data is quite scattered, clear trends can be observed: as β increases, $-\Delta H$ decreases and the mass loss increases. More gaseous products may be produced at a higher heating rate, which may result in a lower $-\Delta H$ value and/or a heat loss due to the production of gases escaping the system.

Table 1 summarizes the experimental results as well as the corrected peak temperatures (T_c) and heating rates (β) used to perform the calculations in the ASTM E698 method. Three correction factors were used to calculate the corrected peak temperatures: temperature scale non-linearity, heating rate changes and thermal lag [13].

Fig. 6 shows the plot of $\ln(\beta T_c^{-2})$ against $1/T_c$, where the slope equals $-E_a/R$. The activation energy, $E_a = 207 \pm 18\,\mathrm{kJ\,mol^{-1}}$, was obtained from the slope of the graph while the log of the pre-exponential factor, $\ln(Z/\mathrm{min^{-1}}) = 47.7 \pm 4.6$, was calculated from the expression given in ASTM E698: $Z = \beta \frac{E}{RT^2} \exp\left(\frac{E}{RT}\right)$.

The above values are consistent with those reported by Geetha et al. [7], who have performed a similar study using heating rates from 10 to 25 °C min^{-1} ($E_a = 199.45\,\mathrm{kJ\,mol^{-1}}$, $\ln(Z/\mathrm{min^{-1}}) = 46.2$).

To complete the ASTM E698 study, isothermal tests were performed on CL-20. Assuming a first-order reaction and using the above values for E_a and $\ln(Z)$, the temperature

Table 1
Dependence of CL-20 DSC results on heating rate (ASTM E698)

Sample mass (mg)	β (°C min^{-1})	Mass loss (%)	T_o[a] (°C)	T_c[b] (°C)	$-\Delta H$ (kJ g^{-1})
0.201	1.01	88.05	202	225.5	3.25
0.205	1.01	89.75	200	223.4	2.85
0.183	2.01	89.60	204	233.1	3.22
0.203	2.01	89.16	203	233.4	2.95
0.193	5.04	92.75	212	243.1	3.16
0.207	5.04	86.47	213	242.8	2.86
0.192	10.02	92.70	216	245.4	2.27
0.201	10.00	94.50	216	246.7	2.61

[a] Onset temperature (first departure from the baseline).
[b] Corrected peak temperature.

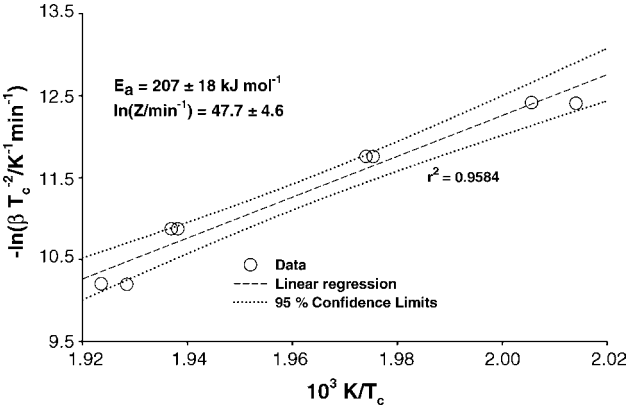

Fig. 6. Kinetic study on the thermal decomposition of CL-20 by DSC.

for a 1 h half-life was calculated as $T_{1/2} = 204\,^{\circ}\mathrm{C}$. Consequently, CL-20 samples of about 0.2 mg were thermally aged at $T_{1/2}$ for 60 min. A mass loss of $54 \pm 10\%$ was observed after these isothermal tests. The samples were then cooled to room temperature, weighed and reheated to 300 °C using $\beta = 5\,^{\circ}\mathrm{C\,min^{-1}}$, and a purge gas flow of 50 mL min^{-1} N_2.

The enthalpy of the aged sample (ΔH_{aged}) should be half that of the unaged sample (H_{unaged}), if the kinetic parameters used to determine $T_{1/2}$ describe the decomposition kinetics correctly. For $\beta = 5\,^{\circ}\mathrm{C\,min^{-1}}$, the overall average enthalpy of decomposition of the aged samples was:

$$\Delta H_{\mathrm{aged}} = -1.5 \pm 0.3\,\mathrm{kJ\,g^{-1}}$$

compared to that obtained with the unaged samples:

$$\Delta H_{\mathrm{unaged}} = -3.0 \pm 0.2\,\mathrm{kJ\,g^{-1}}$$

Since $\Delta H_{\mathrm{aged}} = \frac{1}{2}\Delta H_{\mathrm{unaged}}$, it is concluded that the values of the Arrhenius parameters determined by the ASTM E698 method adequately model the overall kinetics of the decomposition process, even though a multi-step process is clearly evidenced in Fig. 4.

An average of $56 \pm 12\%$ mass loss was calculated after rerunning the aged samples. It should be noted that the onset temperature of the aged samples occurred at about $181 \pm 7\,^{\circ}\mathrm{C}$, which is significantly lower than that of the unaged samples (see Table 1).

3.1.3. Isoconversional data analysis

A model-free kinetic analysis, using the software IsoKin [22], was performed on the results from the DSC heating rate study ($\beta = 1$, 2, 5 and 10 °C min^{-1}). The equations and the procedure used for the analysis are described elsewhere [23]. Fig. 7a shows the calculated dependency of activation energy, E_a, on the extent of reaction, α. The first stage ($0.0 < \alpha < 0.4$) shows constant activation energy ($192 \pm 7\,\mathrm{kJ\,mol^{-1}}$). This observation suggests that the rate-limiting step is unchanged over most of the initial decomposition. For $0.4 \leq \alpha \leq 0.8$, the activation energy varies between about 205 and 265 kJ mol^{-1}. These results are within the 95% confidence limits and agree with those obtained from the ASTM E698 method. The curve in Fig. 7a shows an increase of the activation energy for $0.4 \leq \alpha \leq 0.55$ suggesting the occurrence of parallel reactions [24]. Then, as α increases from 0.55 to 0.80, the activation energy decreases. The graph suggests a complex reaction for the thermal decomposition taking place in the range $0.4 \leq \alpha \leq 0.8$.

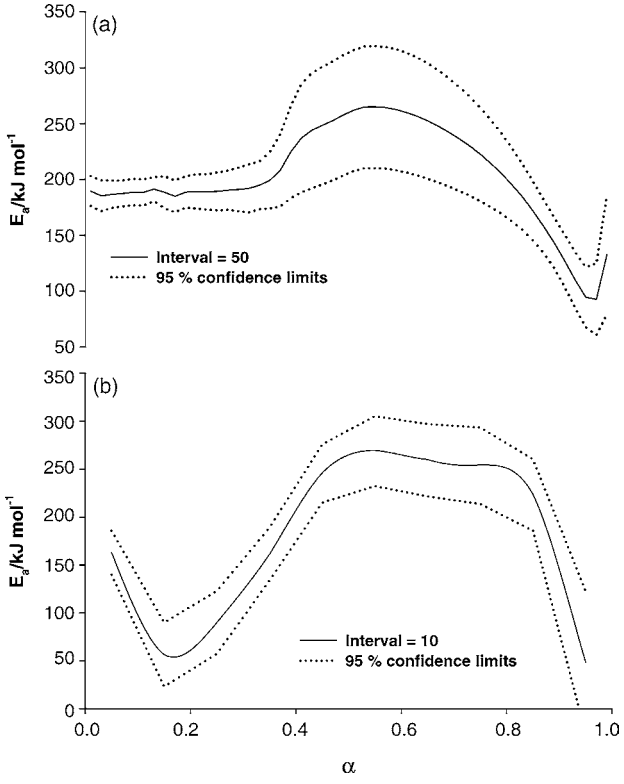

Fig. 7. Result of isoconversional analysis of DSC (a) and TG (b) data: dependence of the activation energy, E_a, on the extent of conversion, α.

3.2. Thermogravimetry (TG)

3.2.1. Thermal behaviour

The TG results for various heating rates are illustrated in Fig. 8. The observed behaviour of the mass loss curves confirms the two-step decomposition noted above in the DSC experiments. An average mass loss of $82 \pm 5\%$ was recorded after the experiments. Fig. 8 also shows that the mass loss of CL-20 increases as the heating rate decreases: slower heating rates give more time for decomposition to occur. It can also be noted that the mass loss from the first decomposition step is generally smaller than that of the second step and generally increases as the heating rate decreases. The rates of decomposition are also different from one another since the slopes of the two parts of the curve are not the same (i.e. first step slope > second step slope).

Comparing Fig. 8 with Fig. 4, it appears that the onset of mass loss observed in the TG experiments occurs at a lower temperature (10–15 °C) than that observed for the onset of exothermic decomposition in the DSC experiments performed at the same heating rate. Additional TG experi-

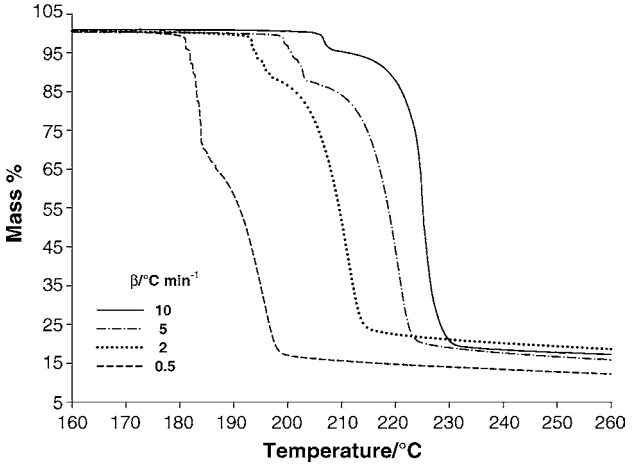

Fig. 8. Thermal decomposition and mass loss at various heating rates by TG.

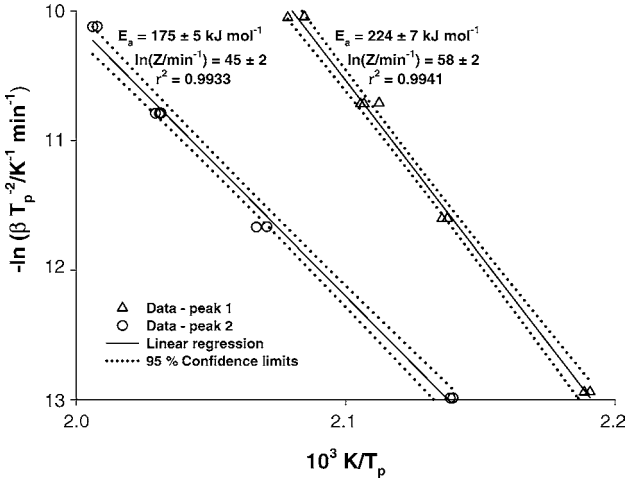

Fig. 9. Kinetic study on the thermal decomposition of CL-20 by TG.

ments performed with both 0.2 and 1 mg samples have shown that only about half of this temperature difference can be attributed to the mass of the sample. This discrepancy may be due to the very different experimental configurations used in these instruments. It should be pointed out that such a discrepancy has already been reported elsewhere for CL-20 [25] and that the data from an earlier study [4] appears to exhibit the same trend. However, as will be seen later, when the experiments are performed under identical conditions (simultaneous TG–DTA), the onset of mass loss and exothermic heat flow are observed to occur at the same temperature.

The TG results obtained at various heating rates were also used to determine the kinetic parameters for the thermal decomposition of CL-20, in accordance with the ASTM E1641 method [16]. Activation energies and pre-exponential factors were derived from the $\ln(\beta)$ versus $1/T$ curves, where T is the temperature at which 30, 40, 50 and 60% conversion was obtained. The kinetic parameters obtained at the various degree of conversion are shown in Table 2. Note that for the kinetic parameters found at 30% conversion, the lowest heating rate ($0.5\,^{\circ}\mathrm{C\,min^{-1}}$) was excluded from the calculations since the second mass loss step occurs around 30% conversion. By comparing the activation energies and the pre-exponential factors at various conversions, it is obvious that the rate of reaction is not constant throughout the decomposition of CL-20. Again, this provides evidence for a multi-step thermal decomposition process.

Similar calculations were performed to determine the activation energy from the maxima of the mass derivative (DTG) curve (Fig. 9) for the first and the second steps. It is seen that the first order kinetic parameters derived for the first peak are higher than the ones for the second peak. The activation energy for the first peak is significantly higher than that for the second peak. Both the activation energy and the slope of the TG curve suggest that the first step of the decomposition proceeds at a lower rate than the second step. This suggests that the first and second peaks follow two different reaction mechanisms.

Table 2
Comparison of kinetic parameters for CL-20 at various degree of conversion in TG experiments

Conversion (%)	E_a (kJ mol^{-1})	ln(Z) (min^{-1})
30	185 ± 6	47 ± 2
40	147 ± 9	37 ± 3
50	166 ± 8	42 ± 2
60	174 ± 9	44 ± 3

3.2.2. Isoconversional data analysis

A model-free kinetic analysis was also performed on the data from the TG heating rate study (0.5, 2, 5 and $10\,^{\circ}\mathrm{C\,min^{-1}}$). The equations and the procedure used for the analysis are described elsewhere [23]. Fig. 7b shows the calculated dependence of activation energy, E_a, on the extent of reaction, α. The graph demonstrates the different stages of the reaction.

The decrease of activation energy from 160 to 55 kJ mol^{-1}, in the range of $0.0 < \alpha \leq 0.15$, suggests that another process is competing with solid phase decomposition in this conversion range. While the nature of this process cannot be inferred from the present data, it is interesting to note that competitive sublimation and condensed-phase exothermic decomposition have been observed for other high performance explosives such as NTO [26].

After this initial decrease, the activation energy starts to increase up to $\alpha \approx 0.45$. This behaviour is similar to that seen in the DSC isoconversional analysis curve (Fig. 7a) and suggests the occurrence of an autocatalytic reaction. The activation energy then stabilizes at about 260 kJ mol^{-1} between $0.45 \leq \alpha \leq 0.85$. These results are within the 95% confidence limits and agree with those obtained from both the DSC isoconversional analysis and the ASTM E698 method. As with the DSC results, the TG isoconversional analysis curve demonstrates the complex reaction scheme occurring during the decomposition of CL-20.

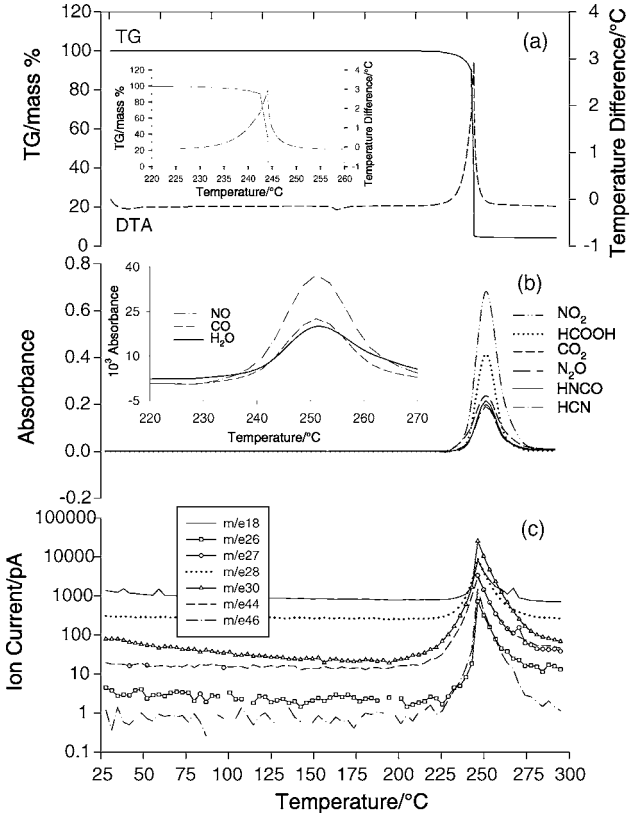

Fig. 10. TG–DTA (a), FTIR (b), and MS (c) results for 5.3317 mg CL-20 heated in helium at 10 °C min^{-1} to 300 °C.

3.3. SDT–FTIR–MS

3.3.1. Thermal behaviour

The thermal decomposition of ∼5 mg of CL-20 was studied by simultaneous SDT–FTIR–MS at various heating rates (2, 5 and 10 °C min^{-1}) with a purge of 50 mL min^{-1} of air or helium. The TG and DTA data for a 10 °C min^{-1} heating rate and a 50 mL min^{-1} helium purge are plotted against the temperature in Fig. 10a. The TG results show a significant mass loss of about 94% at the onset temperature $T_o = 224 \pm 1$ °C along with a strong exothermic reaction illustrated by the DTA trace. Experiments performed in helium and in air gave similar TG–DTA thermal curves and close examination of these curves reveals that the onset of mass loss in the TG curves occurred at the same temperature as the onset of exothermic decomposition in the DTA curves. Many gaseous products were observed from the decomposition of CL-20 as shown in Fig. 10b. NO_2 is the most significant product of the decomposition. It indicates the homolysis of the N–NO_2 bonds [27] from the CL-20 structure, the dominating decomposition reaction. Major traces of N_2O, CO_2, HCOOH and HNCO were identified by FTIR. H_2O, HCN, CO and NO were also detected with very small absorbances. Some of these gases (CO_2, N_2O, NO_2, HCN, NO and CO) were reported in other studies on CL-20 [4,5,26] and result from secondary decomposition reactions. All the peaks from the FTIR coincide with the mass loss and the exotherm observed in the TG–DTA curves. The peaks of the MS curves in Fig. 10c also correspond to the FTIR and TG–DTA peaks. The MS graph shows the evolved gases having a mass to charge ratio (*m*/*e*) of 18 (H_2O), 26 (possibly CN), 27 (HCN), 28 (CO), 30 (NO), 44 (CO_2 and N_2O) and 46 (NO_2). The MS results definitely confirm most of the FTIR traces for both helium and air purges. From both the FTIR and MS results, other carbonaceous gaseous products were also observed to result from the decomposition of CL-20. These include the ions with mass to charge ratio of 26 (42, 48, 54 and 70 are not shown in Fig. 10c since their intensities are weak). The results discussed above are summarized in Table 3 along with the onset temperature and the mass loss of CL-20 for various heating rates and purge gas.

As seen previously in the DSC results, the onset temperature of decomposition increases with the heating rate. Table 3 shows that there is no effect of the purge gas on the onset temperature. The mass loss is however very sensitive to the type of gas used as a purge when heating the sample at either 5 or 2 °C min^{-1}. When air was used as the purge gas, the mass loss noted was about 10% higher than when using a purge of helium. This suggests that formation of the carbonaceous gaseous species reported above is either favoured by the presence of air or these species originate from oxidation of carbonaceous solid residues.

Scaling factors [27] were used to convert the absorbances of some gaseous products (CO_2, N_2O, CO, NO and NO_2) to concentrations relative to CO_2. The results are illustrated in Fig. 11(a) and (b) for He and air purge, respectively. Both graphs show a high concentration of NO_2, the main product of decomposition. In air, the concentration of NO_2 is significantly higher than in helium because NO is converted to NO_2. On the other hand, the concentration of NO in helium is almost twice as high as that observed for the decomposition of CL-20 in air. Therefore, running CL-20 in air increases the concentration of NO_2 and decreases the concentration of

Table 3
Summary of SDT–FTIR–MS non-isothermal results for ∼5 mg CL-20 in 50 mL min^{-1} air or helium

β (°C min^{-1})	Gas	T_o (°C)	Δm (%)	FTIR results	MS results
10	Air	224 ± 1	92 ± 1	H_2O, NO, CO, CO_2, N_2O, NO_2, HCOOH, HNCO, HCN	*m*/*e* 18, 30, 42, 44, 46, 48, 54, 70
10	He	224 ± 1	94 ± 2	H_2O, NO, CO, CO_2, N_2O, NO_2, HCOOH, HNCO, HCN	*m*/*e* 18, 26, 27, 28, 30, 44, 46
5	Air	218 ± 1	98 ± 2	H_2O, CO_2, N_2O, NO_2, HCOOH, HNCO, HCN	*m*/*e* 18, 30, 42, 44, 46
5	He	219 ± 1	80 ± 1	H_2O, NO, CO, CO_2, N_2O, NO_2, HCOOH, HNCO, HCN	*m*/*e* 18, 26, 27, 28, 30, 44, 46
2	Air	210 ± 1	92 ± 2	H_2O, CO, CO_2, N_2O, NO_2, HCOOH, HNCO, HCN	*m*/*e* 18, 30, 42, 44, 46
2	He	211 ± 1	83 ± 1	H_2O, NO, CO, CO_2, N_2O, NO_2, HCOOH, HNCO, HCN	*m*/*e* 18, 26, 27, 28, 30, 44, 46

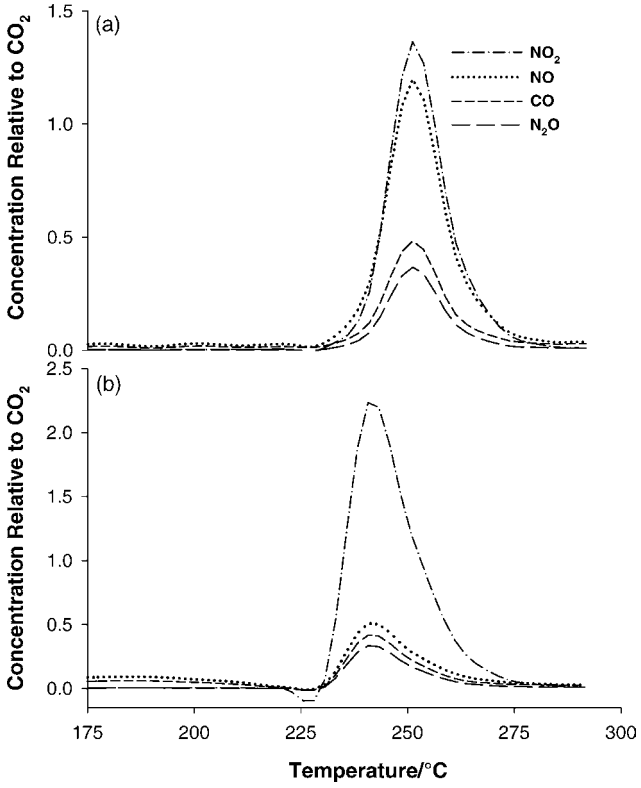

Fig. 11. FTIR results in helium (a) and in air (b) for CL-20 decomposition at 10 °C min^{-1}.

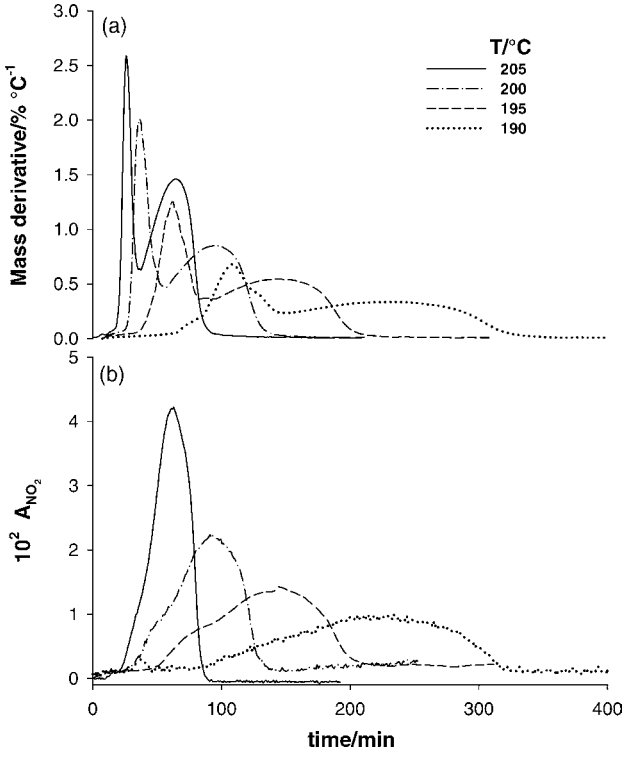

Fig. 12. Time dependence of the mass derivative (a), and NO_2 absorbance (b) in isothermal SDT–FTIR–MS experiments in helium at different temperatures.

NO released during the thermal decomposition. The relative concentrations of N_2O and CO are about the same in both helium and air atmosphere.

3.3.2. Isothermal SDT–FTIR–MS

The thermal decomposition of ~5 mg of CL-20 was also studied by simultaneous SDT–FTIR–MS at various isothermal temperatures (190, 195, 200 and 205 °C) with a flow of 50 mL min^{-1} He. The major products of decomposition resulting from this isothermal study were identified by FTIR (CO_2, N_2O, NO_2 and an unknown carbonaceous product). The mass spectrometer also detected NO, CO_2, N_2O and NO_2.

Using different assumptions, kinetic information can be calculated from these isothermal studies [19,28]. In a first case, if it is assumed that the time, τ, for a particular event to occur is inversely proportional to the rate constant, kinetic parameters can be derived from the corresponding $\ln(\tau)$ against $1/T_{iso}$ plot. Fig. 12a shows the variation of the mass derivative (DTG) as a function of time, for the various isothermal temperatures investigated. Two peaks are clearly observed and the time to the maximum of the DTG peaks (τ_p) is seen to increase as the isothermal temperature decreases. The corresponding $\ln(\tau_p)$ versus $1/T_{iso}$ plot, for each peak, is shown in Fig. 13 together with the kinetic parameters obtained from linear regressions for both DTG peaks.

These isothermal studies also reveal the presence of large amounts of NO_2 in the decomposition products and Fig. 12b shows the variation in NO_2 absorbance (FTIR) with time at various isothermal temperatures. Using the same assumption as above for the isothermal DTG data, kinetic parameters can also be derived using the time to peak NO_2 absorbance obtained from the data of Fig. 12b. The corresponding $\ln(\tau_p)$ versus $1/T_{iso}$ plot and the extracted kinetic parameters are shown in Fig. 14.

Fig. 14 shows a plot of $-\ln(A_{max})$ against $1/T_{iso}$, where A_{max} is the maximum NO_2 absorbance. This plot can be used to derive Arrhenius kinetic parameters, assuming that the re-

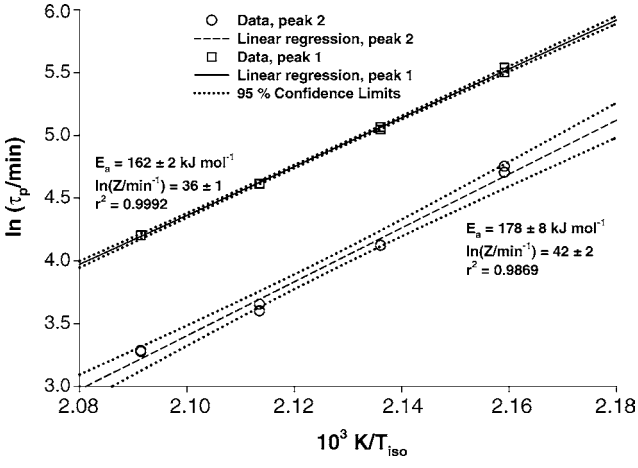

Fig. 13. Plot of ln[time-to-event (τ_p)] vs. $1/T_{iso}$ for DTG data derived from isothermal SDT–FTIR–MS experiments in helium at different temperatures.

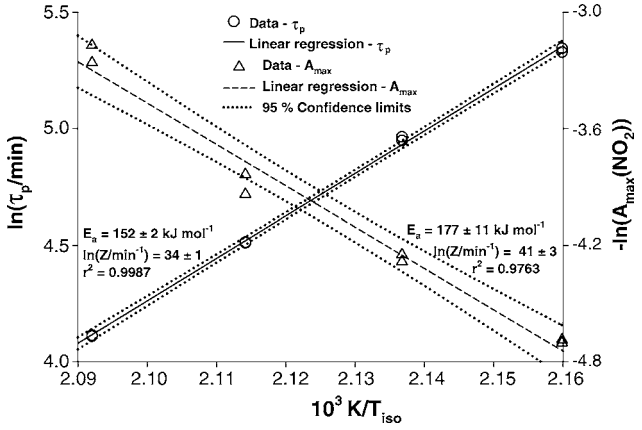

Fig. 14. Plot of ln[time-to-event (τ_p)] and ln[maximum-NO_2-absorbance (A_{max})] vs. $1/T_{iso}$ for NO_2 absorbance data from isothermal SDT–FTIR–MS experiments.

action rate is proportional to the NO_2 concentration. Comparing the Arrhenius parameters obtained from Figs. 13 and 14, it can be seen that the various values for E_a and ln(Z) obtained from these isothermal experiments are quite similar, considering the quoted uncertainties.

3.4. Heat flux calorimetry (HFC)

The modified heat flux calorimeter (HFC) was used to determine the effect of pressure on the thermal decomposition of CL-20. The HFC thermal curves shown in Fig. 15 illustrate the thermal decomposition of CL-20 at ambient (a) and elevated (b) pressure, respectively. Samples of about 50 mg CL-20 were heated from 25 to 300 °C at 0.3 °C min^{-1} under either 0.1 or 7.4 MPa of argon. For both ambient and high pressure runs, a phase transition similar to that observed in the DSC experiments is seen to occur (see insets in Fig. 15). The pressure appears to have only a slight effect on the peak temperatures of the endothermic reaction. For runs in ambient argon, $T_p = 146 \pm 1$ °C, while $T_p = 153 \pm 1$ °C for experiments at 7.4 MPa argon. The endothermic peak is then followed by an exothermic reaction occurring at $T_p = 205 \pm 1$ °C at 0.1 MPa and $T_p = 203 \pm 1$ °C at 7.4 MPa. The results show only a small variation in the exothermic peak temperature with increase in pressure. However, the enthalpy of reaction is significantly higher when the CL-20 is heated under elevated pressure (-4.5 kJ g^{-1} at 7 MPa compared to -3.0 kJ g^{-1} at 0.1 MPa). This could be a chemical effect in which the products catalyze the decomposition or simply a physical effect. After the experiments at both ambient and high pressure, the alumina liners in the vessel were broken into many fragments and a 100% mass loss was recorded. No thermal decomposition studies under pressure could be found in the literature for comparison.

3.5. Accelerating rate calorimetry (ARC)

ARC experiments were conducted to determine the thermal stability of CL-20. Fig. 16 illustrates the variation of

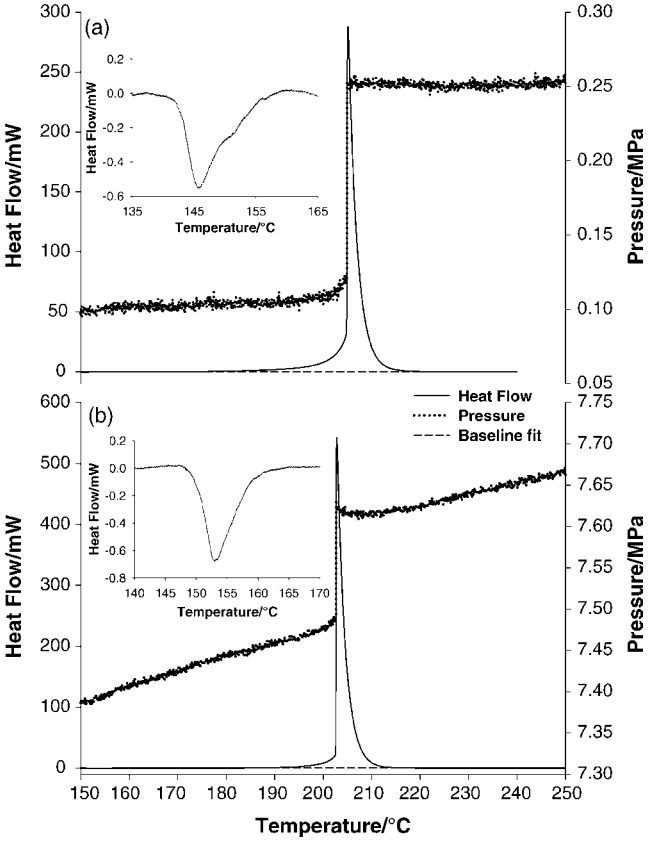

Fig. 15. Study of thermal decomposition and pressure effect on CL-20 by HFC: ~50 mg, 0.3 °C min^{-1}: (a) 0.1 MPa argon; (b) 7.4 MPa argon.

temperature and pressure with time. Under ambient initial pressure of argon, the ARC detected onset temperature is 185 ± 2 °C while the extrapolated onset temperature is 183 ± 2 °C. As shown in Fig. 16 (inset) this extrapolated onset temperature was determined by extrapolating the self-heating rate curve to zero. When the exothermic reaction occurred, the self-heating rate of the sample exceeded 5 °C min^{-1}. A mass loss of 99 ± 1% and a residual pressure of about 0.1 MPa were noted after the runs. The high mass loss contrasts with the low residual pressure and this may be a result of the violent reaction of CL-20 during its thermal decomposition. CL-20

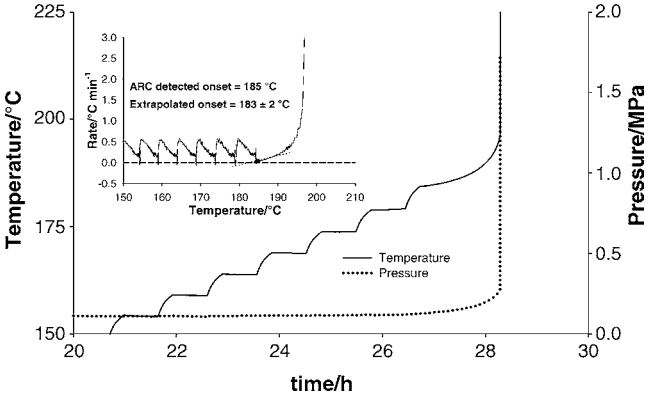

Fig. 16. ARC heat-wait-search results for 0.2 g of CL-20 in ambient argon.

and/or its decomposition products may have condensed in the upper portion of the ARC manifold.

4. Discussion

Table 4 compares the results obtained from all the various sets of experiments. It suggests that the onset temperature of decomposition of CL-20 varies between 172 and 224 °C, depending on the experimental conditions. Since these conditions can be very different from one another, it is expected to observe such a variation in the onset temperature. Most experiments performed in the present work seem to indicate that the second decomposition step may be autocatalytic in nature and this agrees with earlier findings [4,9–12]. It is therefore expected that different experimental conditions may yield different results for the Arrhenius kinetic parameters since these conditions may affect the availability of certain reaction products. As mentioned previously, both the sample size and the heating rate have a significant effect on the results. Some experiments were performed at a heating rate as low as 0.3 °C min^{-1} while other experiments were conducted at 10 °C min^{-1}. The ARC and the HFC experiments were performed in a closed system with rather large free volumes (10 and 29 cm^3, respectively). On the other hand, for TG and SDT–FTIR–MS experiments, the samples were placed in open pans while the DSC experiments were conducted with pinhole pans. The resulting kinetic parameters are therefore somewhat different due to the various assumptions and experimental conditions used. However, the mass loss observed in all the instruments is quite comparable.

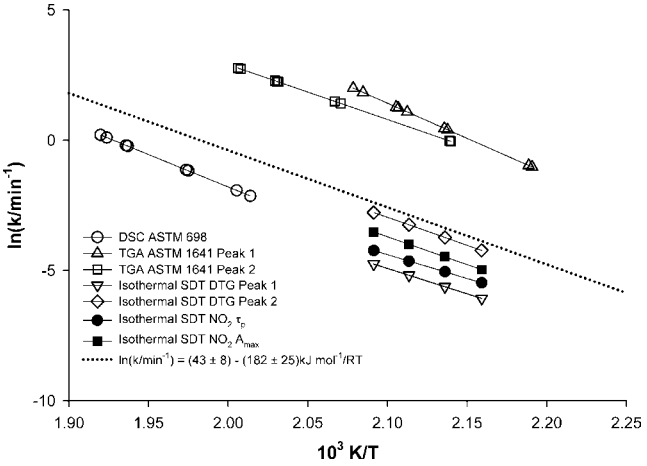

Fig. 17. Arrhenius plots for the thermal decomposition of CL-20 using different methods.

The rate constants calculated from the various measurements are compared in Fig. 17. As mentioned earlier, the kinetic parameters vary significantly with the temperature and the experimental conditions. It is therefore expected to obtain a corresponding variation in the rate constants. However, it should be mentioned that, if one would use the standard deviations quoted in Table 4 to compute the errors associated with the calculated rate constants, one would find that that all the techniques are in agreement with each other within these calculated error bars. The TG results give the highest rate constant while the smallest was obtained from isothermal SDT–DTG experiments. The equation for the rate constant, $\ln(k/\text{min}^{-1}) = (43 \pm 8) - (182 \pm 25)\,\text{kJ mol}^{-1}/RT$ is also plotted in Fig. 17. This equation was obtained using

Table 4
Comparison of onset temperatures, mass losses and kinetic parameters obtained from the various methods used in the present work

System	Gas	T_o (°C)	T_p (°C)	Δm (%)	E_a (kJ mol^{-1})	ln(Z) (min^{-1})
DSC	N_2	212[a]	243[b]	90 ± 3		
ASTM E698					207 ± 18	48 ± 5
IsoKin ($0.4 \le \alpha \le 0.8$)					235 ± 30	
IsoKin ($\alpha < 0.4$)					192 ± 4	
TG	N_2	196[c]	201, 220[d]	82 ± 5		
ASTM E1641 (DTG)					224 ± 7[e], 175 ± 5[f]	58 ± 2[e], 45 ± 2[f]
IsoKin ($0.45 \le \alpha \le 0.85$)					247 ± 23	
TG–DTA–FTIR–MS	He	–	–	82 ± 2		
Isothermal DTG					162 ± 2[e], 178 ± 8[f]	36 ± 1[e], 42 ± 2[f]
Isothermal FTIR (NO_2)					152 ± 2[g], 177 ± 11[h]	34 ± 1[g], 41 ± 3[h]
HFC (C-80)	Ar					
0.1 MPa		172	205	100	–	–
7.4 MPa		183	203	100	–	–
ARC	Ar					
Heat-wait-search		183	–	99 ± 1		

[a] 212 °C is the onset temperature for $\beta = 5$ °C min^{-1}. The onset temperature ranges from 201 to 217 °C for β between 1 and 10 °C min^{-1}, respectively.
[b] 243 °C is the peak temperature for $\beta = 5$ °C min^{-1}. The peak temperature ranges from 224 to 246 °C for β between 1 and 10 °C min^{-1}, respectively.
[c] 196 °C is the onset temperature for $\beta = 5$ °C min^{-1}. The onset temperature ranges from 175 to 203 °C for β between 0.5 and 10 °C min^{-1}, respectively.
[d] 201 and 220 °C are the DTG peak temperatures for $\beta = 5$ °C min^{-1}. The peak temperatures range from 184 to 207 °C for peak 1, and from 196 to 225 °C for peak 2, as β varies from 0.5 to 10 °C min^{-1}.
[e] From analysis of DTG peak 1.
[f] From analysis of DTG peak 2.
[g] From time to peak NO_2 absorbance (τ_p).
[h] From maximum NO_2 absorbance (A_{max}).

the unweighted average of $\ln(Z)$ and E_a from the different experimental studies (Table 4). This expression is therefore recommended to estimate the rate constants for the decomposition of CL-20 over the temperature range 180 and 250 °C, under inert atmosphere. The above average values should be compared to those obtained in previous studies by fitting isothermal TG data for the decomposition of ε-CL-20 with a first order + autocatalytic model. For the autocatalytic part of the reaction the derived E_a and $\ln(Z/\text{min}^{-1})$ values reported were 185 ± 7 [4], 187 ± 12 [9,10], 183.3 ± 0.3 kJ mol^{-1} [12], and 45.5 ± 1.9 [4], 43.9 ± 3.3 [9,10], 45.0 ± 0.1 [12], respectively. These values are in agreement with the above experimental average values, which suggests that, as discussed in [11], the autocatalytic step dominates the overall kinetics.

5. Conclusions

All the experiments performed with the various instruments indicate the multi-step thermal decomposition of CL-20 and its autocatalytic behaviour. Comparable activation energies, pre-exponential factors were derived from the various data analysis and methods. The rate constants calculated from these various sets of kinetic parameters are found to agree to within the stated standard deviations for each measurement. Overall, CL-20 lost about 85% of its initial mass during the decomposition and its onset temperature was found to vary with the heating rate. As CL-20 decomposes, the FTIR and MS detected various gaseous products such as NO_2, N_2O, NO, CO_2, CO, HCN, HCOOH, HNCO, H_2O, as well as other carbonaceous products that could not be identified with the techniques used in the present work. It was determined that the concentration of NO_2 relative to CO_2 was larger than the concentration of all the other gaseous products. From the results obtained using heat flux calorimetry (HFC), it is concluded that the enthalpy of reaction of CL-20 increases with an increase in initial pressure. While this is also consistent with an autocatalytic process, this could also reflect a change in the reaction mechanism.

References

[1] H. Bazaki, S. Kawabe, H. Miya, Propell. Explos. Pyrotech. 23 (1998) 333.
[2] K. Jun-Hyung, Y. Yoo-Jin, J. Chem. Eng. Jpn. 32 (1999) 237.
[3] M.J. Mezger, S.M. Nicolich, D.A. Geiss Jr., R.L. Hatch, K.E. Lee, Proceedings of the 30th International Annual Conference of ICT, Karlsruhe, Federal Republic of Germany, 1999.
[4] S. Löbbecke, M.A. Bohn, A. Pfeil, H. Krause, Proceedings of the 29th International Annual Conference of ICT, Karlsruhe, Federal Republic of Germany, 1998.
[5] T.P. Russel, P.J. Miller, G.J. Piermarini, S. Block, J. Phys. Chem. 97 (1993) 1993.
[6] M.F. Foltz, C.L. Coon, F. Garcia, A.L. Nichols III, Propell. Explos. Pyrotech. 19 (1994) 133.
[7] M. Geetha, U.R. Nair, D.B. Sarwade, G.M. Gore, S.N. Asthana, H. Singh, J. Therm. Anal. Calorim. 73 (2003) 913.
[8] D.G. Patil, T.B. Brill, Combust. Flame 87 (1991) 145.
[9] B. Korsounskii, V. Nedelko, N. Chukanov, T. Larikova, Proceedings of the 30th International Annual Conference of ICT, Karlsruhe, Federal Republic of Germany, 1999.
[10] B.L. Korsounskii, V.V. Nedel'ko, N.V. Chukanov, T.S. Larikova, F. Volk, Russian Chem. Bull. 49 (2000) 812.
[11] V.V. Nedelko, N.V. Chukanov, A.V. Raevskii, B.L. Korsounskii, T.S. Larikova, O.I. Kolesova, Propell. Explos. Pyrotech. 25 (2000) 255.
[12] M.A. Bohn, Propell. Explos. Pyrotech. 27 (2002) 1125.
[13] ASTM E698, American Society for Testing Materials, West Conshohocken, PA, USA.
[14] ASTM E967, American Society for Testing Materials, Conshohocken, PA, USA.
[15] ASTM E968, American Society for Testing Materials, Conshohocken, PA, USA.
[16] ASTM E1641-99, American Society for Testing Materials, Conshohocken, PA, USA.
[17] ASTM E1582, American Society for Testing Materials, Conshohocken, PA, USA.
[18] ASTM E2040, American Society for Testing Materials, Conshohocken, PA, USA.
[19] D.E.G. Jones, P.D. Lightfoot, R.C. Fouchard, Q. Kwok, A.-M. Turcotte, W. Ridley, Thermochim. Acta 384 (2002) 57.
[20] D.E.G. Jones, A.-M. Turcotte, R.C. Fouchard, Thermochim. Acta 401 (2003) 63.
[21] ASTM E1981–98, American Society for Testing Materials, Conshohocken, PA, USA.
[22] C.A. Wight, Isoconversional Data Analysis Program, Version 1.42, Center of Thermal Analysis, University of Utah, 2000.
[23] S. Vyazovkin, J. Comput. Chem. 18 (1997) 393.
[24] M.E. Brown, Handbook of Thermal Analysis and Calorimetry, Elsevier, Amsterdam, Netherlands, 1998.
[25] NIMIC Database, Data Sheet for Hexanitrohexaazaisowurtzitane, February 21, 2003, MSIAC Secure Internet Website: Munitions Safety Information Analysis Center (MSIAC). http://www.nato.int/related/nimic.
[26] G.T. Long, B.A. Brems, C.A. Wight, J. Phys. Chem. B 106 (2002) 4022.
[27] T.B. Brill, H. Arisawa, P.J. Brush, P.E. Gongwer, G.K. Williams, J. Phys. Chem. 99 (1995) 1384.
[28] R.L. Blaine, S.M. Marcus, J. Therm. Anal. 49 (1997) 1485.